Supplement of

Seasonal Variation of Oxygenated Organic Molecules (OOMs) and its Contribution to Secondary Organic Aerosol (SOA) in Urban Beijing

Yishuo Guo et al.

Correspondence to: Chao Yan (chao.yan@helsinki.fi)

Section S1. Estimation of OOM Volatility

Detailed structure information of OOMs in real atmosphere is still unknown, therefore, the volatility of each OOM molecule was estimated based on a parameterization using numbers of different atoms (Donahue et al., 2011). For the oxidation products from monoterpenes, previous studies show that except from hydroxyl (-OH), carbonyl (-C=O) and carboxyl (-C(O)OH) groups, hydroperoxide (-OOH) also takes a large portion (Tröstl et al., 2016;Stolzenburg et al., 2018). Then by assuming that all nitrogen atoms exist as organonitrate groups ($-ONO_2$), the saturation mass concentration of OOM molecule at 300 K can be given as follows (Tröstl et al., 2016):

$$\log_{10}C^{*}(300K) = (25 - nC) \cdot bC - (nO - 3nN) \cdot bO - 2 * \left[\frac{(nO - 3nN) \cdot nC}{nC + nO - 3nN}\right] \cdot bCO - nN \cdot bN$$

where nC, nO and nN are the numbers of carbon, oxygen, and nitrogen in each molecule respectively, and bC=0.475, bO=0.2, bCO=0.9, and bN=2.5. For oxidation products from aromatics, the work of Mingyi Wang et al. shows that they possess more -OH and -C=O groups as well as less hydroperoxides, and that their estimated saturation concentrations suggested by Donahue et al. (Donahue et al., 2011) match well with the experiment ones (Wang et al., 2020). Therefore, for those non-monoterpene OOMs, the estimation from Donahue et al. was applied:

$$\log_{10}C^{*}(300K) = (25 - nC) \cdot bC - nO_{eff} \cdot bO - 2 * \left(\frac{nC \cdot nO_{eff}}{nC + nO_{eff}}\right) \cdot bCO$$

where nC, nO_{eff} and nN are the numbers of carbon, effective oxygen and nitrogen in each molecule separately, and bC=0.475, bO=2.3, and bCO=-0.3.

The temperature dependence of C^{*} is given by the Clausius-Clapeyron equation (Epstein et al., 2010;Donahue et al., 2012), which we can be approximated as:

$$\log_{10}C^{*}(T) = \log_{10}C^{*}(300K) + \frac{\Delta H_{vap}}{R\ln(10)}\left(\frac{1}{300} - \frac{1}{T}\right)$$

where the evaporation enthalpy ΔH_{vap} can be linked with $\log_{10}C^{*}(300K)$ according to the following equation:

$$\Delta H_{vap}[\mathrm{kJ\ mol^{-1}}] = -5.7 \cdot \log_{10}C^{*}(300K) + 129$$

After the temperature related saturation concentrations were calculated, OOMs were then grouped into different bins based on the volatility basis set (VBS) (Donahue et al., 2006), and further classified as ELVOCs (extremely low volatility organic compounds), LVOCs (low volatility organic compounds), SVOCs (semi-volatile organic compounds), IVOCs (intermediate volatility organic compounds) and VOCs (volatile organic compounds) according to their volatilities (Donahue et al., 2012).

Section S2. Simulation of OOM Net Condensation Flux

An aerosol growth model was used to calculate the OOM net condensation flux onto particles (Tröstl et al., 2016;Stolzenburg et al., 2018). This model is based on the VBS distribution mentioned above, and each VBS bin is regarded as a single surrogate species with the averaged mass and concentration.

The condensation flux, $\emptyset_{i,p}$, of low volatile OOMs at each moment can be simulated as:

$$\emptyset_{i,p} = N_p \cdot \sigma_{i,p} \cdot k_{i,p} \cdot F_{i,p}$$

where N_p, $\sigma_{i,p}$, $k_{i,p}$ and $F_{i,p}$ are the particle number concentration at a given size (p), the particle-vapor collision cross-section between each VBS bin (i) and a given particle size (p), the deposition rate of OOM vapor at the particle surface, and the driving force of condensation respectively. $\sigma_{i,p}$ is derived from the particle diameter d_p and vapor diameter d_i as:

$$\sigma_{i,p} = \pi/4(d_p + d_i)^2$$

The deposition rate of OOMs, $k_{i,p}$, depends on the center mass velocity of particle and vapor $v_{i,p}$, the mass accommodation coefficient $\alpha_{i,p}$, and the non-continuum dynamic factor $\beta_{i,p}$:

$$k_{i,p} = \alpha_{i,p} v_{i,p} \beta_{i,p}$$

where $v_{i,p} = \sqrt{\frac{8RT}{\pi\mu_{i,p}}}$, is the average velocity for Maxwell's velocity distribution law. $\mu_{i,p}$ is the reduced mass and is defined as $\frac{M_i M_p}{M_i + M_p}$.

The driving force of condensation is defined as:

$$F_{i,p} = C_i^0(S_i - a'_{i,p})$$

where C_i^0, S_i and $a'_{i,p}$ are the saturation vapor concentration, saturation ratio and particle phase activity of each VBS bin, respectively. The excess saturation ratio $S_i^{XS} = S_i - a'_{i,p}$ is the key diagnostic for condensation. $a'_{i,p}$ accounts for particle mixture effect with Raoult term $X_{i,p}\gamma_{i,p}$ and curvature effect with Kelvin term $K_{i,p}$ as:

$$a'_{i,p} = X_{i,p}\gamma_{i,p}K_{i,p}$$

where $X_{i,p}$ is the mass fraction of organic compounds of each VBS bin (i) in the condensed phase at given particle size (p), and $\gamma_{i,p}$ is the mass based activity coefficient in the condensed phase. In this study, $\gamma_{i,p} = 1$ was used with the assumption of ideal solution. The Kelvin term, $K_{i,p} = \exp\left(\frac{4\sigma_p M_i}{RT\rho_p D_p}\right)$, is related to surface tension σ_p, molar weight M_i and density ρ_p.

For OOMs with relatively higher volatility (i.e., C_i^*>0.1 μg m^{-3}), their partitioning between the gas and condensed phase will likely reach equilibrium when the condensation and evaporation of OOMs are approximately equal. Then the fraction of species i in condensed phase, f_i^{aer}, can be described by the aerosol partition theory (Seinfeld and Pandis, 2016) as:

$$f_i^{aer} = \frac{1}{1 + C_i^*/C_{OA}^{aer}} = \frac{C_i^{aer}}{C_i}$$

where C_i^*, C_i, C_{OA}^{aer}, and C_i^{aer} are the effective saturation concentration of the OOMs vapor in each VBS bin, total mass concentration of species i in the gas and condensed phase, total mass concentration of organic aerosol, and mass concentration of species i in the condensed phase.

The seasonal variations of OOM condensation fluxes for low volatility OOMs (ELVOCs and LVOCs) and high volatility OOMs (SVOCs, IVOCs and VOCs) are shown in Fig. S12 (A) and (B) respectively. It can be found that, compared with low volatility OOMs, the condensation flux of high volatility OOMs is minor, and the net flux of them onto particles are zero over a period of time. Consequently, the rate of OOMs condensing onto particles could be approximately estimated based on the condensation of ELVOCs and LVOCs.

According to the above model, the condensation flux is mainly influenced by the oversaturation of OOMs and the surface area of aerosols ($Area_{aero}$). Since ELVOCs and LVOCs undergo almost irreversible condensation (Ehn et al., 2014), their gas phase concentration is nearly the same as their oversaturated concentration. Therefore, we further looked into the relationship between condensation flux and ELVOC and LVOC concentration ([ELVOCs+LVOCs]) times $Area_{aero}$. Results in Fig. S13 show that they have perfect linear correlation in all four seasons. The slope in the figure represents the ability of ELVOCs and LVOCs forming SOA through condensation, to be more specific, the amount of SOA produced through condensation by unit concentration of ELVOCs and LVOCs (1 $\mu g/m^3$) under unit aerosol surface concentration (1 m^2/m^3) in an hour. This condensation ability of ELVOCs and LVOCs is quite stable during the year (6.3-8.4 $m^2 \cdot m^{-3} \cdot h$). And its influencing factors are possibly particle composition, concentration of gaseous vapors and the interaction between vapors and particle surface.

Section S3. Definition of Characteristic Accumulation Time

The characteristic accumulation time (AccTime), which is introduced for roughly comparison of SOA formation rates from OOM condensation among different seasons, is defined as:

$$\mathrm{AccTime} = \frac{[\mathrm{SOA}]}{[\mathrm{CondenFlux}]_{\mathrm{ELVOC+LVOC}}}$$

where [SOA] is the mass concentration of SOA in $\mu g \cdot m^{-3}$, and $[\mathrm{CondenFlux}]_{\mathrm{ELVOC+LVOC}}$ is the mass condensation flux of OOMs in $\mu g \cdot m^{-3} \cdot h^{-1}$, and therefore, AccTime is in the unit of hour.

In real atmosphere, there are various SOA sources. So this AccTime should not be interpreted as that SOA is entirely formed from OOM condensation within this characteristic time, but only a straightforward estimation of how fast SOA is formed if its source only comes from OOM condensation.

FIGURES

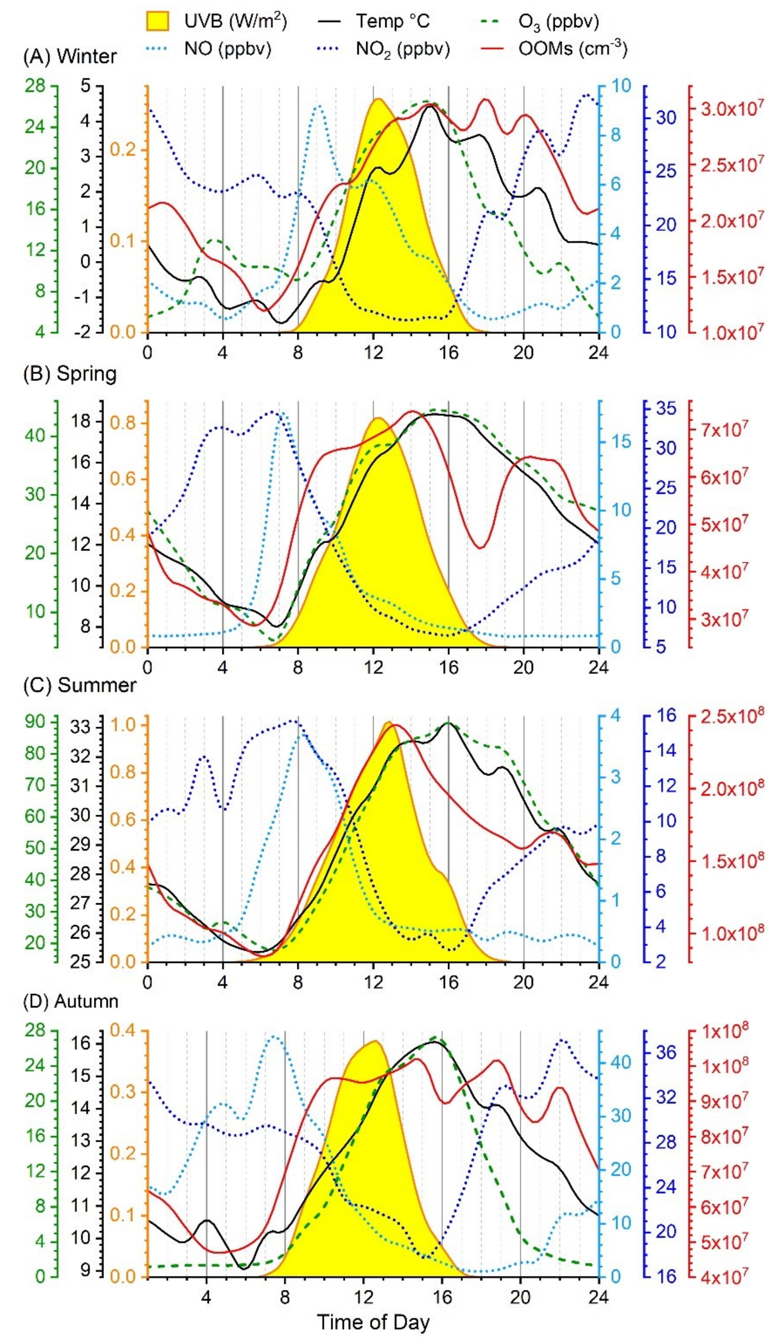

Figure S1. Diurnals variations of UVB, temperature (Temp), mixing ratio of O_3, NO and NO_2, and OOM concentration in four seasons.

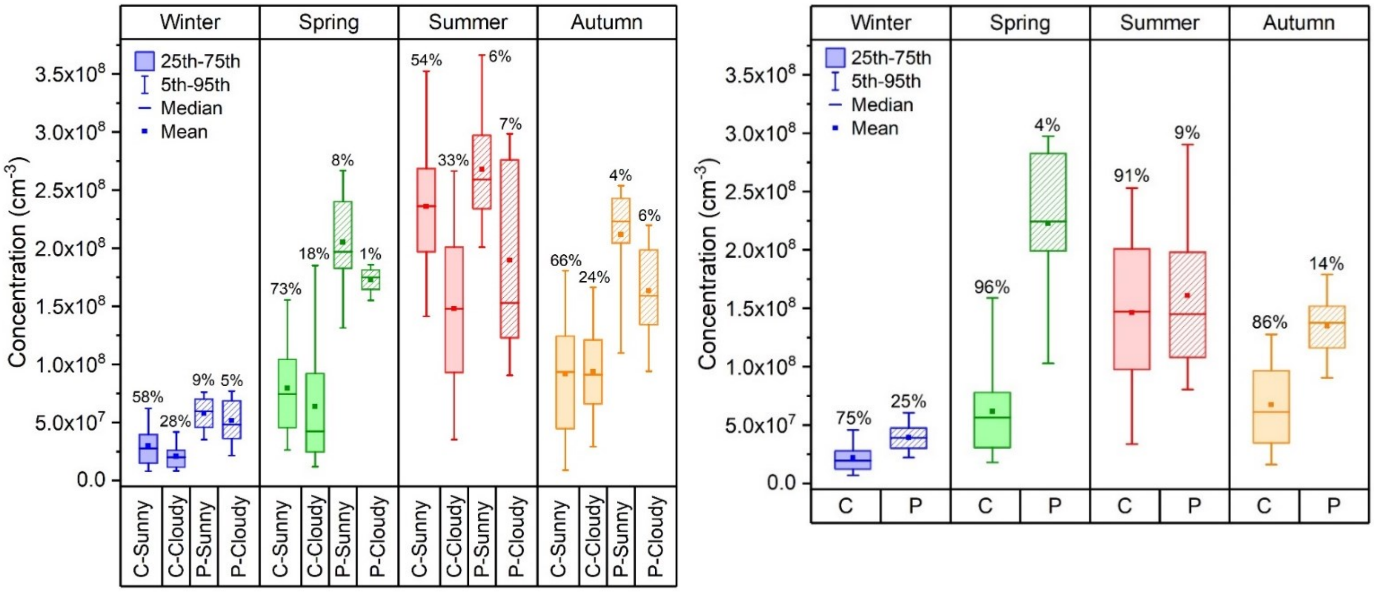

Figure S2. Left panel: Concentration of total OOMs in four seasons under different atmospheric conditions during daytime (08:00-16:00). The abbreviations "C" and "P" represent clean and polluted condition respectively. Clean and polluted conditions are divided by $PM_{2.5}$ with a value of 75 μg/m^3. Sunny and cloudy day are distinguished by brightness parameter (Dada et al., 2017) with a value of 0.5. The percentages are fractions taken up by each condition in each season. Right panel: Concentration of total OOMs in four seasons under different atmospheric conditions during nighttime (20:00-04:00 next day). The abbreviations "C" and "P" represent clean and polluted respectively. Those two conditions are divided by $PM_{2.5}$ with a value of 75 μg/m^3. The percentages are fractions taken up by each condition in each season.

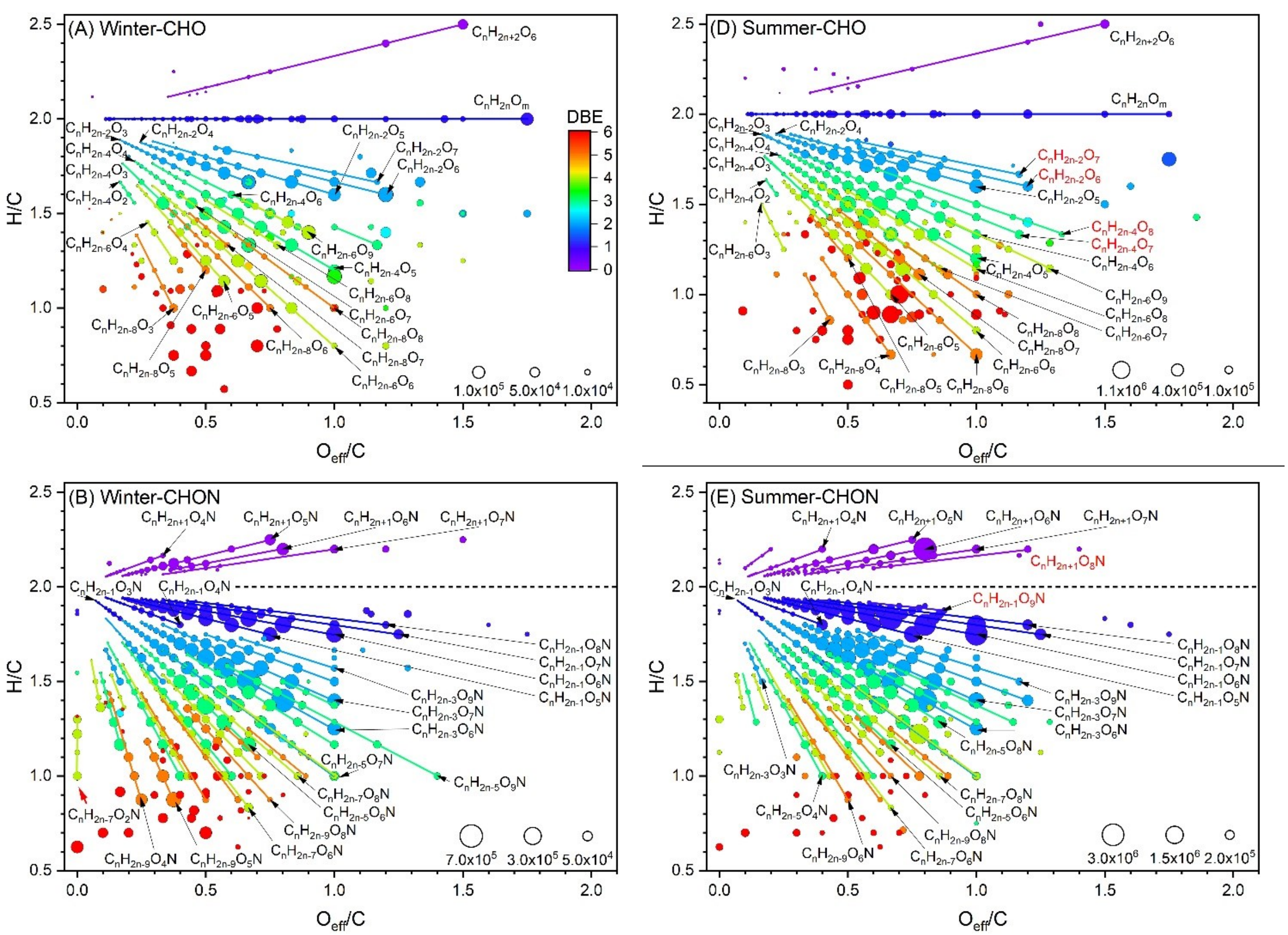

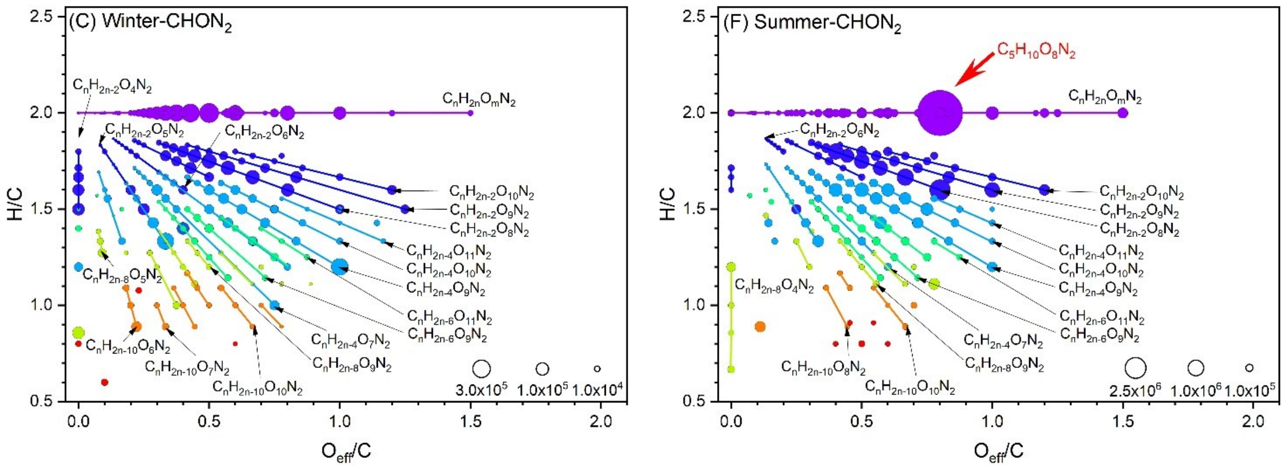

Figure S3. The ratio of hydrogen number to carbon number (H/C) against the corresponding ratio of effective oxygen number to carbon number (O_{eff}/C) for (A) winter CHO OOMs, (B) winter CHON OOMs, (C) winter $CHON_2$ OOMs, (D) summer CHO OOMs, (E) summer CHON OOMs, and (F) summer $CHON_2$ OOMs. The size relates to the concentration of each OOMs molecules. CHO OOMs are those only contain carbon, hydrogen and oxygen atoms. CHON OOMs and $CHON_2$ OOMs are those contain additional one and two nitrogen atoms respectively.

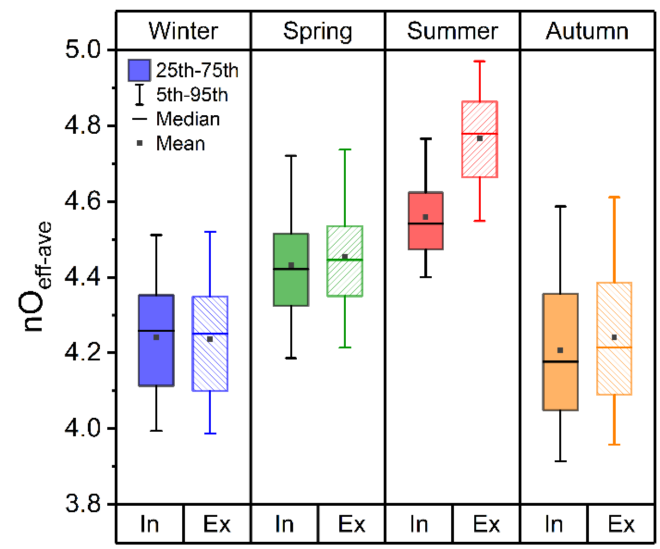

Figure S4. Concentration weighted average number of effective oxygen ($nO_{eff\text{-}ave}$) in four seasons. The abbreviations "In" and "Ex" represent the averaged values for OOMs with and without IP-derived OOMs respectively.

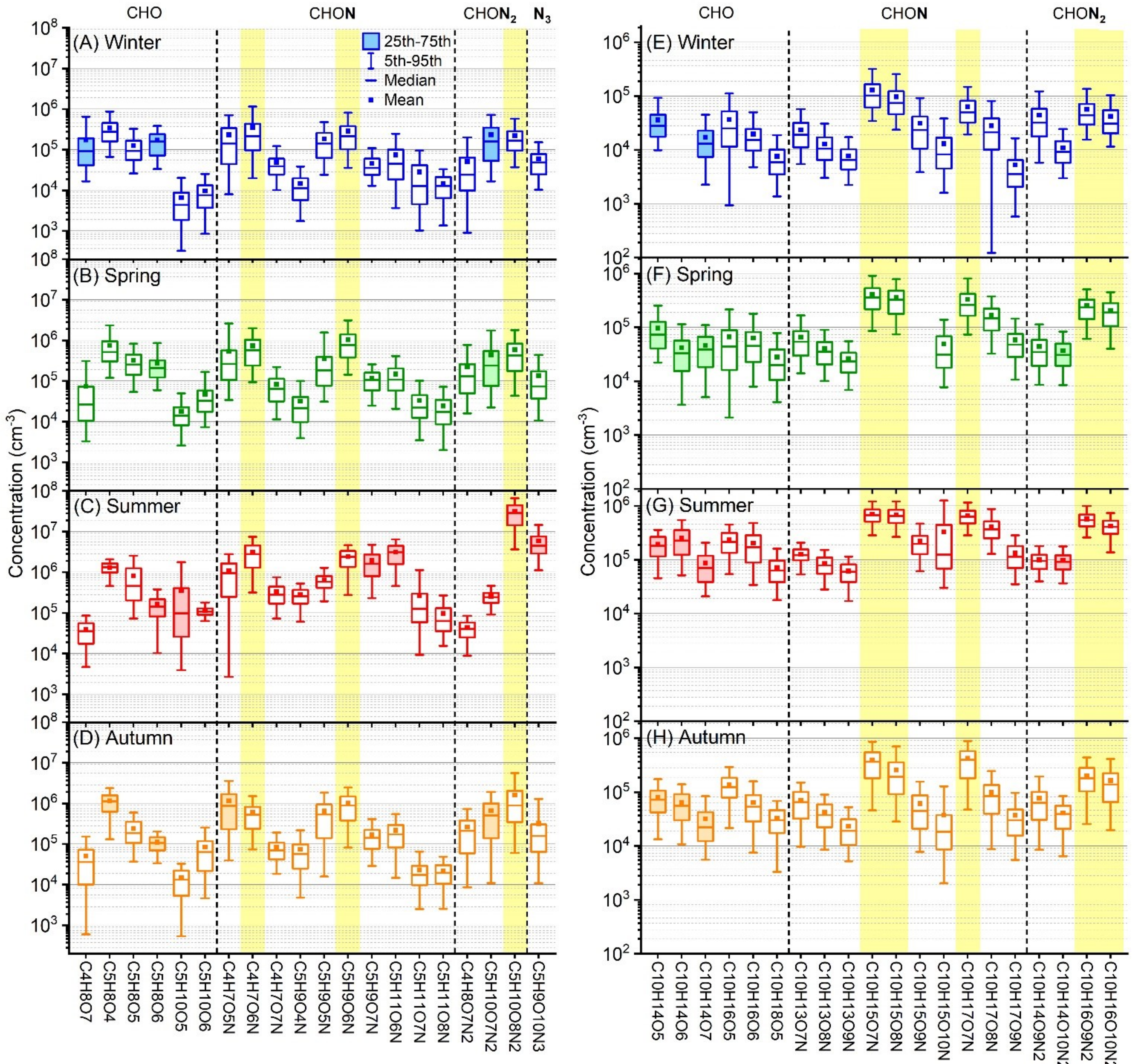

Figure S5. Concentration of typical IP OOMs in (A) winter, (B) spring, (C) summer and (D) autumn, and typical MT OOMs in (E) winter, (F) spring, (G) summer and (H) autumn. Species in grey background are distinct ones in different seasons. Compounds in yellow background are primary ones during the year. The filled boxes are special compounds in each season.

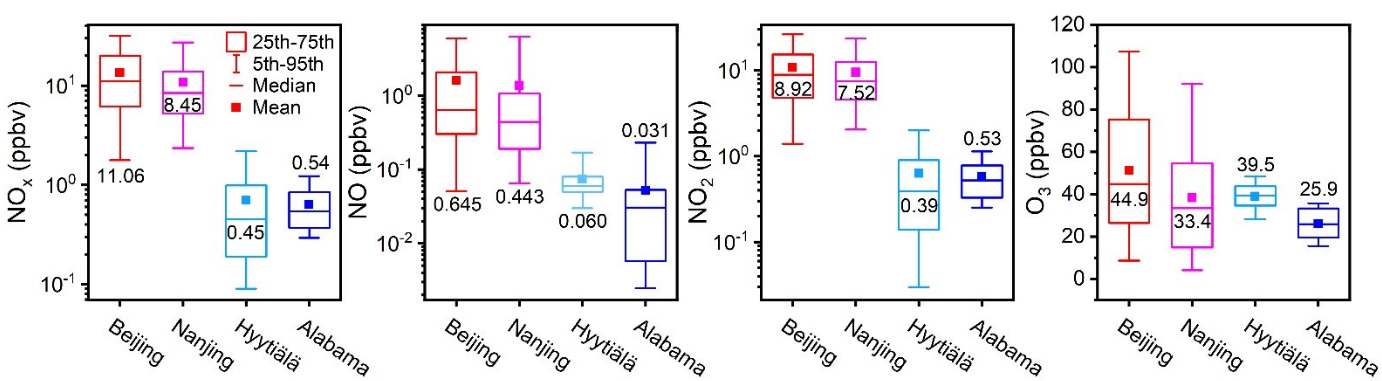

Figure S6. NO_x, NO, NO_2 and O_3 mixing ratios in summer Beijing, summer Nanjing (Liu et al., 2021), spring Hyytiälä (Yan et al., 2016) and summer Alabama (Massoli et al., 2018).

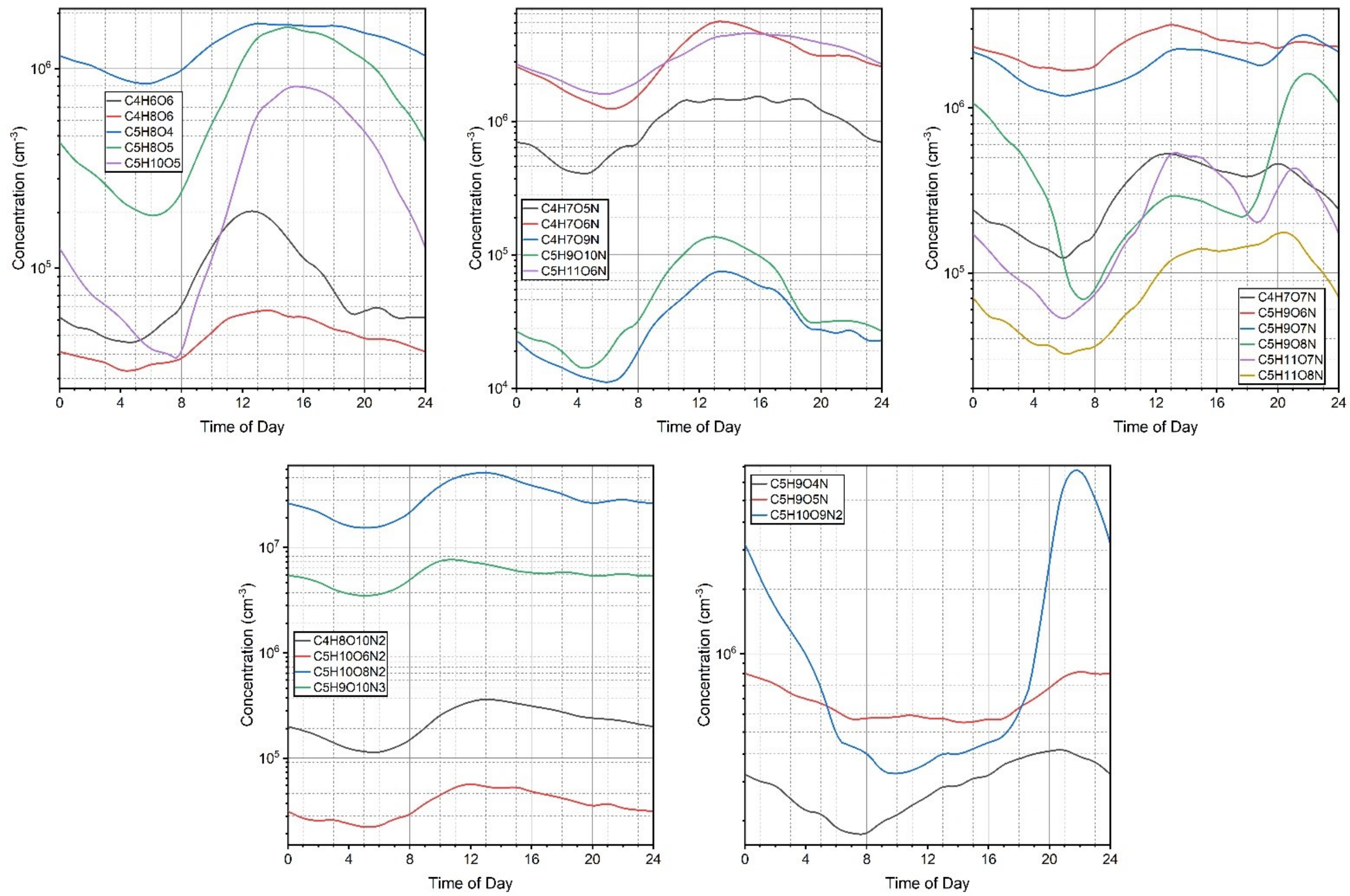

Figure S7. Diurnal variations of representative isoprene OOMs during summertime in this study.

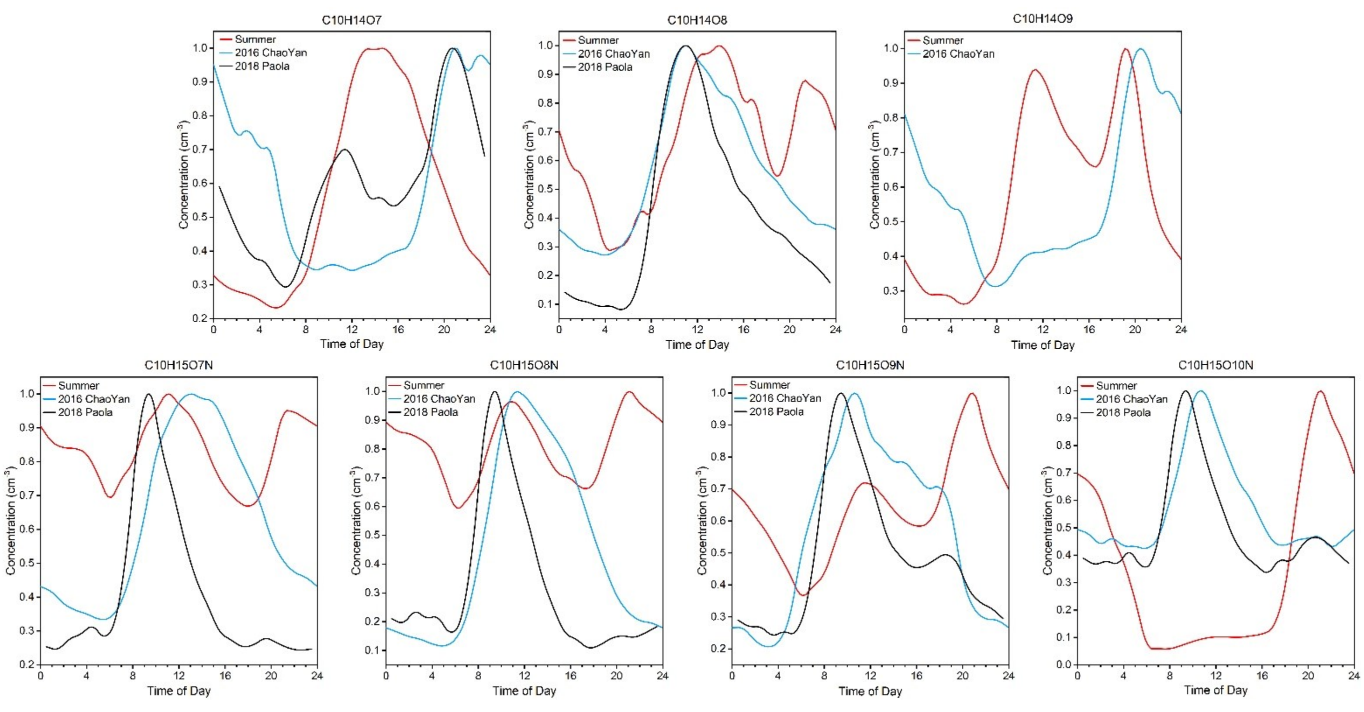

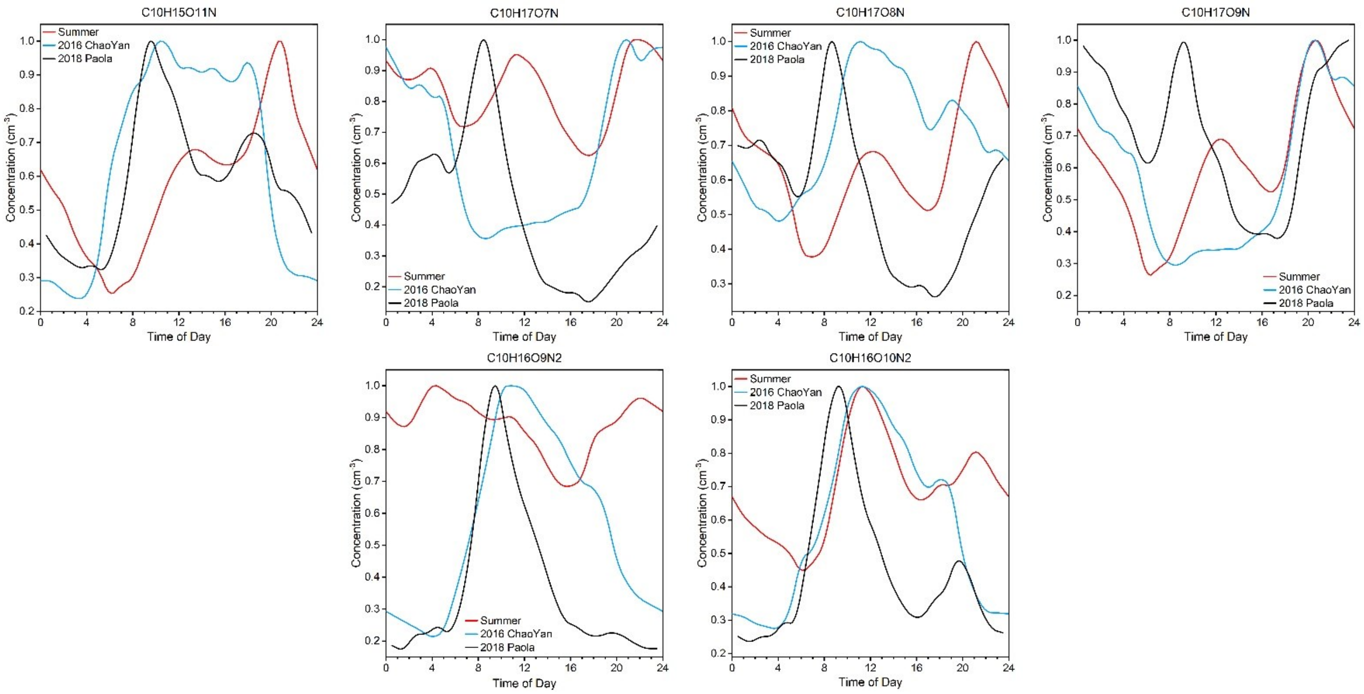

Figure S8 Diurnal variation of representative monoterpene OOMs during summertime in our study and from other two reported forest sites (Yan et al., 2016;Massoli et al., 2018).

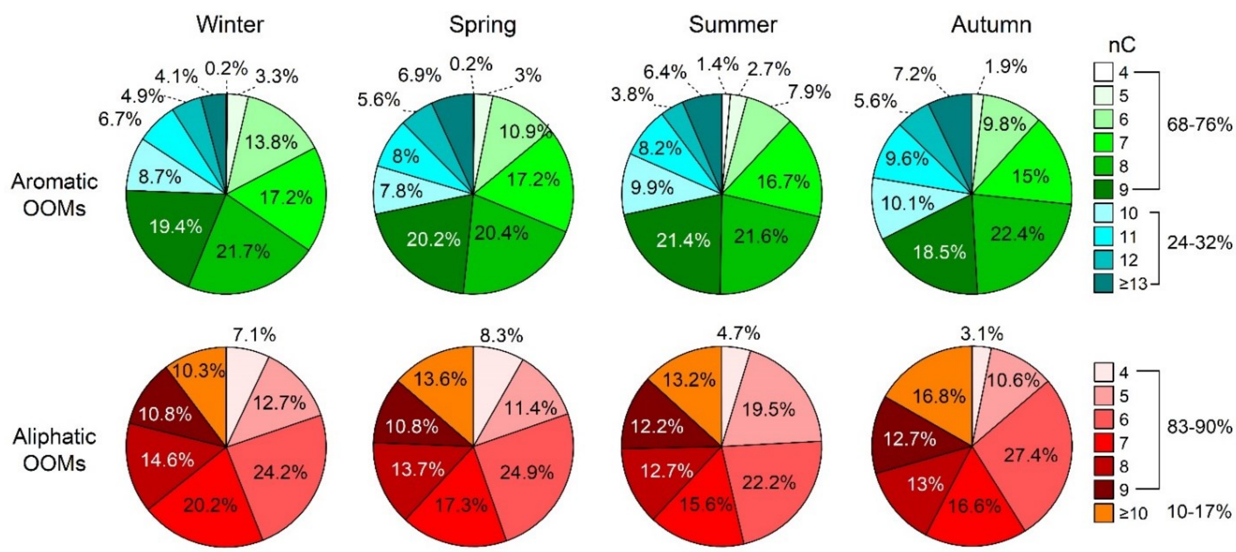

Figure S9. Fractions of aromatic (first row) and aliphatic (second row) OOMs with different number of carbon atoms (nC) in winter (first column), spring (second column), summer (third column) and autumn (forth column). Colors in green, blue, red and orange series are for monocyclic aromatic OOMs (nC≤9), polycyclic aromatic OOMs (nC≥10), short-chain aliphatic OOMs (nC≤9) and long-chain aliphatic OOMs (nC≥10) respectively.

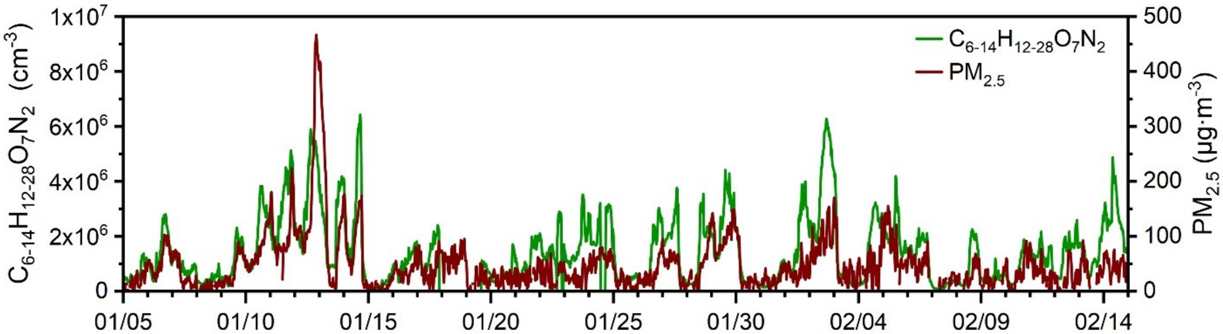

Figure S10. Time variation of $C_{6\text{-}14}H_{12\text{-}28}O_7N_2$ OOMs and $PM_{2.5}$ in winter.

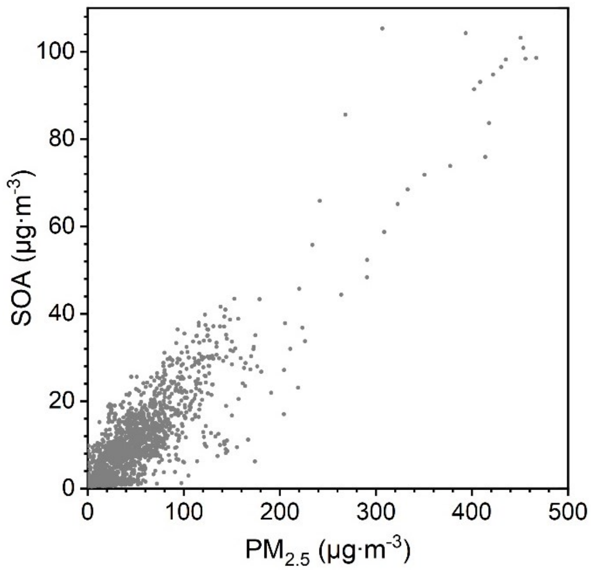

Figure S11. Correlation of SOA with $PM_{2.5}$ in winter.

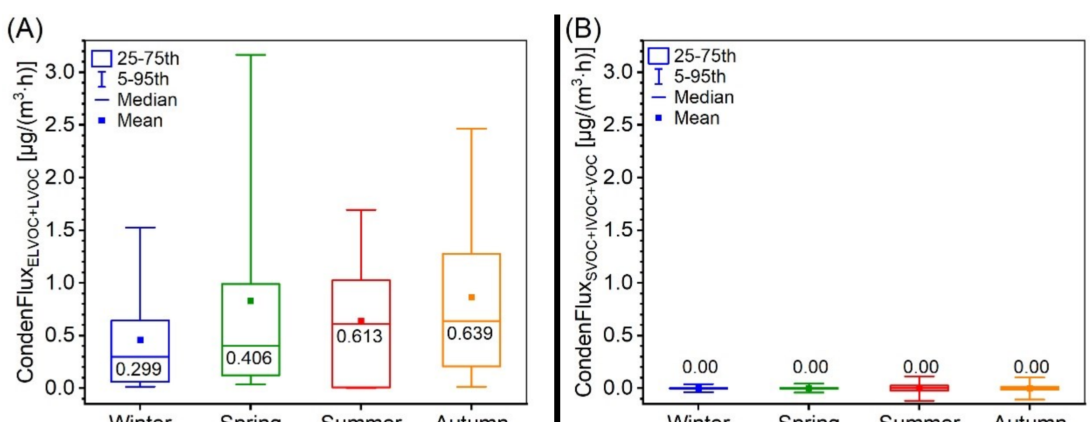

Figure S12. Condensation fluxes of (A) low volatility OOMs (ELVOCs and LVOCs) estimated by the particle dynamic model (Tröstl et al., 2016), and (B) high volatility OOMs (SVOCs, IVOCs and VOCs) calculated based on the aerosol partition theory (Seinfeld and Pandis, 2016) in four seasons**.** The values in each box are the median values.

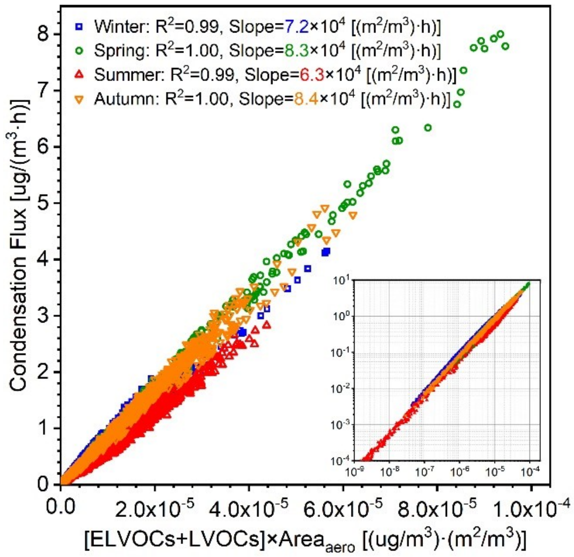

Figure S13. Relationship between OOM condensation flux and concentration of ELVOCs and LVOCs ([ELVOCs+LVOCs]) times aerosol surface area ($Area_{aero}$). The figure inserted is in log scale.

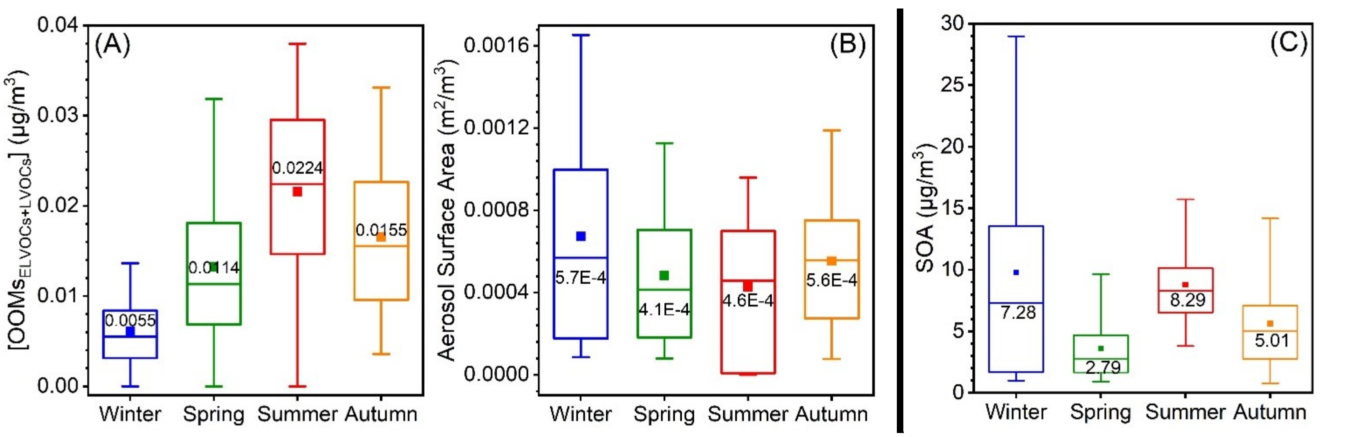

Figure S14. (A) Mass concentration of ELVOCs and LVOCs, (B) aerosol surface area in four seasons and (C) mass concentration of secondary organic aerosol (SOA) in four seasons. The values in each box are the median values of corresponding parameters.

TABLES

Table S1. Median values of UVB, temperature (Temp), relative humidity (RH), O_3, NO, NO_2, condensation sink (CS), organic aerosol (OA) and secondary organic aerosol (SOA) in four seasons. Please note that note that UVB only includes daytime values from 08:00 to 16:00.

Median Values	UVB (W/m^2)	Temp (°C)	RH (%)	O_3 (ppbv)	NO (ppbv)	NO_2 (ppbv)	CS (s^{-1})	SOA ($\mu g/m^3$)	OA ($\mu g/m^3$)
Winter	0.133	0.4	27	14.2	2.6	20.7	0.023	15.33	7.28
Spring	0.467	12.9	27	31.1	1.3	14.6	0.018	6.80	2.79
Summer	0.536	28.6	76	44.9	0.6	8.9	0.020	13.43	8.29
Autumn	0.176	12.1	65	7.2	10.0	28.3	0.023	11.14	5.01

Table S2. Mean, standard deviation (Std), median, 25 and 75 percentiles (25^{th} and 75^{th}) of total OOMs concentration in four seasons under different atmospheric conditions during daytime (08:00-16:00).

Season	Condition	Mean (cm^{-3})	Std (cm^{-3})	Median (cm^{-3})	25^{th} (cm^{-3})	75^{th} (cm^{-3})
Winter	Clean & Sunny	3.0×10^7	1.7×10^7	2.8×10^7	1.5×10^7	4.0×10^7
	Clean & Cloudy	2.1×10^7	1.1×10^7	2.0×10^7	1.1×10^7	2.6×10^7
	Polluted & Sunny	5.8×10^7	1.5×10^7	6.0×10^7	4.6×10^7	7.0×10^7
	Polluted & Cloudy	5.2×10^7	1.9×10^7	4.8×10^7	3.6×10^7	6.9×10^7
Spring	Clean & Sunny	7.9×10^7	4.1×10^7	7.5×10^7	4.5×10^7	1.0×10^8
	Clean & Cloudy	6.5×10^7	5.3×10^7	4.3×10^7	2.6×10^7	9.2×10^7
	Polluted & Sunny	2.1×10^8	4.1×10^7	2.0×10^8	1.8×10^8	2.4×10^8
	Polluted & Cloudy	1.7×10^8	1.3×10^7	1.8×10^8	1.6×10^8	1.8×10^8
Summer	Clean & Sunny	2.4×10^8	6.1×10^7	2.4×10^8	2.0×10^8	2.7×10^8
	Clean & Cloudy	1.5×10^8	6.7×10^7	1.5×10^8	9.3×10^7	2.0×10^8
	Polluted & Sunny	2.7×10^8	5.4×10^7	2.6×10^8	2.3×10^8	3.0×10^8
	Polluted & Cloudy	1.9×10^8	8.2×10^7	1.5×10^8	1.2×10^8	2.8×10^8
Autumn	Clean & Sunny	9.2×10^7	5.6×10^7	9.3×10^7	4.5×10^7	1.2×10^8
	Clean & Cloudy	9.4×10^7	3.7×10^7	9.1×10^7	6.7×10^7	1.2×10^8
	Polluted & Sunny	2.1×10^8	4.1×10^7	2.2×10^8	2.1×10^8	2.4×10^8
	Polluted & Cloudy	1.6×10^8	4.2×10^7	1.6×10^8	1.3×10^8	2.0×10^8

Table S3. Mean, standard deviation (Std), median, 25 and 75 percentiles (25^{th} and 75^{th}) of source-classified OOM concentrations in four seasons.

Season	OOMs Type	Mean (cm^{-3})	Std (cm^{-3})	Median (cm^{-3})	25th (cm^{-3})	75th (cm^{-3})
Winter	IP OOMs	2.4×10^6	1.8×10^6	1.9×10^6	9.6×10^5	3.2×10^6
	MT OOMs	1.4×10^5	8.6×10^5	1.1×10^6	7.3×10^5	1.8×10^6
	Aromatic OOMs	1.0×10^7	6.2×10^6	8.7×10^6	5.3×10^6	1.4×10^7
	Aliphatic OOMs	1.1×10^7	7.7×10^6	8.9×10^6	4.6×10^6	1.4×10^7
Spring	IP OOMs	5.2×10^6	4.5×10^6	3.8×10^6	1.9×10^6	6.8×10^6
	MT OOMs	4.2×10^6	2.6×10^6	3.5×10^6	2.3×10^6	5.3×10^6
	Aromatic OOMs	2.8×10^7	1.9×10^7	2.4×10^7	1.4×10^7	3.5×10^7
	Aliphatic OOMs	2.5×10^7	2.2×10^7	1.9×10^7	9.7×10^6	3.3×10^7
Summer	IP OOMs	5.5×10^7	3.3×10^7	5.3×10^7	2.7×10^7	7.8×10^7
	MT OOMs	8.5×10^6	2.8×10^6	8.4×10^6	6.6×10^6	1.0×10^7
	Aromatic OOMs	4.7×10^7	2.0×10^7	4.7×10^7	3.2×10^7	6.2×10^7
	Aliphatic OOMs	4.3×10^7	1.7×10^7	4.3×10^7	3.2×10^7	5.3×10^7
Autumn	IP OOMs	8.3×10^6	6.8×10^6	7.4×10^6	3.1×10^6	1.1×10^7
	MT OOMs	5.1×10^6	3.1×10^6	4.9×10^6	2.6×10^6	7.1×10^6
	Aromatic OOMs	3.0×10^7	1.7×10^7	2.8×10^7	1.7×10^7	4.1×10^7
	Aliphatic OOMs	3.4×10^7	2.3×10^7	3.2×10^7	1.5×10^7	4.9×10^7

Table S4. Nighttime OH radical and NO_3 radical concentration from previously studies in Beijing.

Measurement Site	Time Period	Radical Conc (cm^{-3})	Reference	Used Radical Conc (cm^{-3})
		OH radical		
Wangdu, Beijing, rural	2014 June	5×10^5	(Tan et al., 2017)	3×10^5
Huairou, Beijing, suburban	2016 Jan.-Mar.	$2 - 4 \times 10^5$	(Tan et al., 2018)	
Peking University, Beijing, urban	2017 Nov.-Dec.	$1 - 4 \times 10^5$	(Ma et al., 2019)	
		NO_3 radical		
Peking University, Beijing, urban	2016 May-June	$3 - 7 \times 10^8$ (calculated)	(Wang et al., 2018)	5×10^8

Table S5. Estimated nighttime loss rate of precursor VOCs from OH radical or NO_3 radical ($Loss_{VOC\text{-}radical}$). $k_{VOC\text{-}radical}$ is the reaction rate of VOC with OH or NO_3 radical.

VOC Type	$k_{VOC\text{-}radical}$ ($cm^3\ s^{-1}$)	Reference	Used Radical Conc (cm^{-3})	$Loss_{VOC\text{-}radical}$ (s^{-1})
		OH radical		
Aromatics	1.2×10^{-12} - 5.7×10^{-11}	IUPAC MCM v3.3.1 (Atkinson and Arey, 2003)	3×10^5	3.6×10^{-7} - 1.7×10^{-5}
Aliphatics	4.6×10^{-17} - 2.4×10^{-12}			1.4×10^{-11} - 7.2×10^{-7}
Monoterpenes	5.2 - 9.3×10^{-11}			1.6 - 2.8×10^{-5}
Isoprene	9.7×10^{-11} – 1.2×10^{-10}			2.9 - 3.7×10^{-5}
		NO_3 radical		
Aromatics	$< 3.0 \times 10^{-17}$ - 1.9×10^{-15}	IUPAC MCM v3.3.1 (Atkinson and Arey, 2003)	5×10^8	$< 1.5 \times 10^{-8}$ – 4.5×10^{-7}
Aliphatics	1.1×10^{-17} – 1.3×10^{-16}			2.5×10^{-9} – 6.5×10^{-8}
Monoterpenes	2.5 - 7.7×10^{-12}			1.3 – 3.9×10^{-3}
Isoprene	5.3 - 7.0×10^{-13}			2.7 – 3.5×10^{-4}

Table S6 Fractions of typical IP OOM molecules in total IP OOMs.

Formula	Winter	Spring	Summer	Autumn
		CHO		
C4H8O7	4.58%	0.63%	0.07%	0.53%
C5H8O4	13.80%	12.42%	2.69%	16.76%
C5H8O5	4.70%	6.03%	0.94%	2.74%
C5H8O6	7.90%	5.03%	0.29%	1.54%
C5H10O5	0.22%	0.33%	0.20%	0.20%
C5H10O6	0.38%	0.79%	0.22%	0.93%
C5H12O6	0.85%	0.58%	0.03%	0.45%
		CHON		
C4H7O5N	7.16%	6.27%	1.95%	12.95%
C4H7O6N	10.75%	13.68%	5.70%	7.64%
C4H7O7N	1.95%	1.54%	0.58%	1.02%
C5H9O4N	0.57%	0.51%	0.53%	0.85%
C5H9O5N	7.10%	4.43%	1.20%	7.86%
C5H9O6N	10.76%	18.24%	4.90%	13.04%
C5H9O7N	1.78%	2.57%	3.33%	2.07%
C5H11O6N	2.24%	2.59%	6.40%	2.54%
C5H11O7N	0.64%	0.52%	0.26%	0.26%
C5H11O8N	0.65%	0.41%	0.13%	0.29%
		$CHON_2$		
C4H8O7N2	1.23%	3.11%	0.08%	3.10%
C5H10O7N2	8.02%	5.75%	0.50%	7.46%
C5H10O8N2	8.41%	10.26%	58.21%	13.06%
C5H10O9N2	NaN	NaN	0.89%	0.57%
		$CHON_3$		
C5H9O10N3	2.42%	1.76%	9.26%	2.34%

Table S7 Fractions of typical MT OOM molecules in total MT OOMs.

Formula	Winter	Spring	Summer	Autumn
		CHO		
C10H14O4	2.3%	1.2%	1.4%	1.8%
C10H14O5	2.7%	2.2%	2.3%	1.9%
C10H14O6	NaN	1.0%	2.9%	1.5%

C10H14O7	1.2%	1.3%	0.9%	0.5%
C10H16O4	2.3%	1.5%	1.7%	2.8%
C10H16O5	2.7%	1.3%	2.8%	2.6%
C10H16O6	1.5%	1.5%	2.2%	1.4%
C10H18O4	2.2%	1.5%	1.2%	2.1%
C10H18O5	0.6%	0.6%	0.9%	0.8%
		CHON		
C10H13O6N	1.4%	1.0%	0.6%	1.3%
C10H13O7N	1.8%	1.7%	1.6%	1.6%
C10H13O8N	1.0%	1.1%	1.0%	0.9%
C10H13O9N	0.6%	0.7%	0.8%	0.4%
C10H15O6N	10.7%	7.7%	8.4%	12.5%
C10H15O7N	9.9%	10.6%	8.6%	9.3%
C10H15O8N	7.3%	9.6%	8.7%	5.5%
C10H15O9N	2.5%	NaN	2.5%	1.3%
C10H17O6N	8.4%	5.6%	7.0%	11.2%
C10H17O7N	5.2%	7.7%	8.1%	10.2%
C10H17O8N	2.6%	4.3%	4.7%	2.0%
C10H17O9N	0.4%	1.4%	1.5%	0.8%
		$CHON_2$		
C10H12O8N2	0.7%	0.4%	NaN	0.3%
C10H12O9N2	0.7%	0.4%	0.3%	0.3%
C10H12O10N2	0.3%	0.2%	NaN	0.2%
C10H14O8N2	0.7%	0.8%	0.9%	0.8%
C10H14O9N2	2.3%	1.1%	1.2%	1.4%
C10H14O10N2	0.9%	1.0%	1.2%	0.9%
C10H16O8N2	3.5%	8.7%	6.3%	9.7%
C10H16O9N2	4.3%	7.0%	6.9%	3.1%
C10H16O10N2	3.1%	5.7%	5.2%	3.4%

Table S8 Fractions of typical aromatic OOM molecules in total aromatic OOMs.

Formula	**Winter**	**Spring**	**Summer**	**Autumn**	**(Garmash et al., 2020)**	**(Molteni et al., 2018)**
			CHO			
C5H4O5	0.10%	0.29%	0.17%	0.18%	×	×
C5H4O6	0.17%	0.16%	NaN	NaN	√	×
C5H6O5	0.90%	1.16%	0.72%	0.68%	×	√
C5H7O6	0.73%	0.44%	0.38%	0.17%	×	×
C6H6O4	NaN	0.76%	0.43%	0.80%	√	√
C6H6O5	0.90%	0.81%	0.26%	0.37%	√	√
C6H8O4	1.96%	1.41%	1.32%	2.18%	√	√
C6H8O5	1.29%	1.41%	0.93%	0.94%	√	√
C6H8O6	NaN	0.41%	0.31%	0.27%	√	√
C6H8O7	0.54%	0.24%	0.26%	0.11%	√	√
C7H8O4	0.98%	0.54%	0.64%	0.90%	√	√
C7H8O5	1.52%	1.33%	1.74%	0.96%	√	√
C7H8O6	0.33%	0.24%	0.12%	0.10%	√	√
C7H10O3	0.16%	0.09%	0.12%	0.38%	√	×
C7H10O4	1.47%	1.43%	2.06%	2.24%	√	√
C7H10O5	1.12%	1.48%	1.37%	1.11%	√	√
C7H10O6	0.18%	0.29%	0.66%	0.44%	√	√
C7H10O7	0.11%	0.08%	0.18%	0.27%	√	√
C7H10O8	0.08%	0.08%	0.08%	0.07%	√	√
C7H12O6	0.26%	0.20%	0.16%	0.05%	√	√
C7H12O7	0.12%	0.12%	NaN	0.07%	√	√
C8H10O3	0.30%	0.10%	NaN	0.16%	no xylene experiment	×
C8H10O4	0.72%	0.42%	0.51%	0.77%		√

C8H10O5	1.41%	1.37%	1.54%	1.35%	no C9 aromatic hydrocarbon experiment	√
C8H12O3	0.24%	0.08%	0.08%	0.27%		×
C8H12O4	1.51%	1.91%	2.17%	2.77%		√
C8H12O5	0.97%	0.94%	1.92%	0.93%		√
C8H12O6	0.73%	0.66%	0.71%	0.56%		√
C8H12O7	NaN	0.19%	0.22%	0.11%		√
C8H12O8	NaN	0.15%	0.17%	0.15%		√
C8H14O6	NaN	0.13%	0.23%	0.01%		√
C8H14O7	NaN	0.07%	0.10%	0.11%		√
C9H12O4	NaN	0.18%	0.45%	0.51%		×
C9H12O5	0.72%	0.51%	0.70%	0.44%		×
C9H12O6	NaN	0.19%	0.43%	0.45%		√
C9H12O7	0.24%	0.15%	0.67%	0.08%		×
C9H14O3	1.23%	0.28%	0.19%	0.55%		×
C9H14O4	0.85%	0.61%	0.67%	1.02%		×
C9H14O5	0.64%	0.87%	0.92%	0.77%		√
C9H14O6	0.46%	0.33%	0.65%	0.34%		√
C9H14O7	NaN	NaN	0.26%	0.11%		√
C9H16O6	NaN	0.09%	0.20%	0.10%		×
C9H16O7	NaN	0.08%	0.10%	0.12%		√
C10H14O2	NaN	0.01%	0.02%	0.02%	×	no C10 aromatic hydrocarbon experiment
C10H14O3	0.16%	0.05%	0.03%	0.11%	×	
CHON						
C5H5O4N	0.41%	0.28%	0.19%	0.34%	√	no NO_x experiment
C5H5O5N	0.32%	0.20%	0.09%	0.19%	√	
C5H5O7N	0.48%	0.43%	0.29%	0.11%	×	
C5H7O8N	NaN	NaN	0.75%	0.21%	√	
C6H5O6N	0.38%	0.22%	0.09%	0.14%	√	
C6H7O3N	1.00%	0.42%	NaN	0.06%	×	
C6H7O4N	0.69%	0.48%	0.31%	0.73%	×	
C6H7O5N	0.66%	0.31%	0.13%	0.39%	√	
C6H7O6N	1.71%	1.10%	0.47%	0.90%	×	
C6H7O7N	0.23%	0.19%	0.58%	0.35%	√	
C6H7O8N	0.28%	0.18%	NaN	NaN	√	
C6H9O8N	0.38%	0.27%	0.44%	0.24%	×	
C6H9O9N	NaN	NaN	0.19%	NaN	√	
C7H7O5N	0.25%	0.14%	0.14%	0.27%	no toluene + NO_x experiment	
C7H7O6N	0.47%	0.15%	0.28%	0.29%		
C7H7O7N	0.26%	0.14%	NaN	NaN		
C7H7O8N	0.17%	0.17%	0.13%	0.07%		
C7H7O9N	0.15%	0.14%	0.17%	0.06%		
C7H9O5N	0.77%	0.35%	0.21%	0.49%		
C7H9O6N	2.31%	1.93%	1.25%	1.97%		
C7H9O7N	1.13%	1.38%	1.83%	0.92%		
C7H9O8N	0.34%	1.01%	1.12%	0.27%		
C7H9O9N	0.09%	NaN	0.15%	0.05%		
C7H9O10N	NaN	NaN	0.17%	0.06%		
C7H11O8N	0.50%	0.49%	0.71%	0.27%		
C7H11O9N	0.16%	0.21%	0.22%	0.18%		
C8H9O5N	0.28%	0.26%	0.27%	0.36%	no xylene experiment	
C8H9O6N	0.30%	0.22%	0.20%	0.25%		
C8H9O7N	0.34%	0.38%	0.22%	0.14%		
C8H9O8N	0.09%	0.20%	0.09%	0.04%		
C8H9O9N	0.18%	0.15%	0.16%	0.08%		
C8H11O5N	0.41%	0.18%	0.14%	0.27%		
C8H11O6N	3.88%	2.03%	0.71%	3.38%		
C8H11O7N	1.30%	1.61%	2.87%	1.50%		

C8H11O8N	1.11%	1.58%	1.53%	0.77%		
C8H11O9N	0.25%	0.34%	0.21%	0.14%		
C8H11O10N	0.20%	0.16%	0.13%	NaN		
C8H13O8N	0.58%	0.65%	0.89%	0.51%		
C8H13O9N	NaN	NaN	0.37%	0.10%		
C8H13O10N	0.07%	0.10%	0.17%	0.06%		
C9H11O5N	0.13%	0.14%	0.11%	0.14%		
C9H11O6N	0.31%	0.23%	0.17%	0.19%		
C9H11O7N	0.35%	0.38%	0.27%	0.15%		
C9H11O8N	0.16%	0.24%	0.20%	0.08%		
C9H11O9N	0.14%	0.19%	NaN	0.12%		
C9H11O10N	0.06%	0.32%	0.13%	0.04%		
C9H13O5N	0.29%	0.13%	0.15%	0.24%		
C9H13O6N	2.71%	1.20%	0.69%	2.22%	no C9 aromatic hydrocarbon experiment	
C9H13O7N	1.40%	1.15%	1.86%	1.28%		
C9H13O8N	1.56%	1.67%	1.61%	0.99%		
C9H13O9N	0.43%	0.49%	0.40%	0.18%		
C9H13O10N	0.12%	0.19%	0.18%	0.12%		
C9H15O8N	0.51%	0.72%	1.27%	0.51%		
C9H15O9N	0.14%	0.23%	0.36%	0.15%		
C9H15O10N	NaN	0.20%	0.18%	NaN		
			$CHON_2$			
C8H10O8N2	0.11%	0.11%	0.05%	0.10%		
C8H10O9N2	NaN	NaN	0.19%	NaN		
C8H10O10N2	0.24%	0.18%	0.23%	0.16%		
C8H10O11N2	0.07%	0.07%	0.10%	0.03%	no xylene experiment	
C8H12O10N2	0.22%	0.48%	1.01%	0.48%		
C8H12O11N2	0.04%	NaN	0.15%	0.07%		
C8H12O12N2	0.08%	0.04%	0.05%	0.03%		no NO_x experiment
C9H12O8N2	0.14%	0.14%	0.15%	0.05%		
C9H12O9N2	NaN	0.48%	0.25%	0.16%		
C9H12O10N2	0.22%	0.24%	0.26%	0.14%	no C9 aromatic hydrocarbon experiment	
C9H12O11N2	0.06%	NaN	0.12%	0.04%		
C9H14O10N2	0.27%	0.58%	0.90%	0.47%		
C9H14O11N2	0.03%	0.10%	0.16%	0.10%		
Sum	54.99%	50.31%	53.93%	48.51%	——	——

Table S9 Fractions of DBE≤4 and DBE>4 compounds for nC≤9 and nC≥10 aromatic OOMs in four seasons.

OOM Type	Winter	Spring	Summer	Autumn
		nC≤9 aromatic OOMs		
DBE≤4	83%	80%	83%	84%
DBE>4	17%	20%	17%	16%
		nC≥10 aromatic OOMs		
DBE≤4	34%	32%	41%	33%
DBE>4	66%	68%	59%	67%

Table S10 Fractions of typical aliphatic OOM molecules in total aliphatic OOMs.

Formula	Winter	Spring	Summer	Autumn
		CHO		
C6H10O4	1.68%	1.82%	1.55%	2.31%
C7H12O4	1.05%	1.23%	1.16%	1.58%
C8H14O4	0.50%	0.73%	0.55%	0.92%
C9H16O4	0.41%	0.67%	0.51%	1.04%
		CHON		
C5H7O6N	7.60%	7.50%	7.52%	4.67%
C6H9O6N	8.65%	6.40%	3.63%	6.82%
C6H11O5N	1.86%	0.84%	0.97%	2.39%

C6H11O6N	2.56%	4.59%	6.96%	5.44%
C7H11O5N	1.08%	0.52%	0.34%	0.96%
C7H11O6N	5.69%	5.05%	3.53%	3.92%
C7H13O5N	1.06%	0.50%	0.51%	1.37%
C7H13O6N	1.46%	2.09%	2.37%	1.38%
C7H13O7N	0.30%	0.46%	0.47%	0.30%
C8H13O6N	3.06%	2.41%	2.01%	2.72%
C8H15O5N	0.87%	0.27%	0.40%	0.83%
C8H15O6N	1.15%	1.58%	1.68%	1.13%
C8H15O7N	0.27%	0.52%	0.68%	0.25%
C8H17O5N	0.59%	0.25%	0.17%	0.75%
C9H15O5N	1.01%	0.25%	0.17%	0.38%
C9H15O6N	1.51%	2.66%	2.76%	2.79%
C9H17O5N	0.67%	0.29%	0.36%	0.94%
C9H17O6N	0.86%	1.46%	2.21%	1.35%
C9H17O7N	0.20%	0.92%	0.47%	0.36%
C10H17O5N	0.44%	0.19%	0.18%	0.74%
C10H17O6N	1.05%	1.08%	1.28%	1.71%
C10H19O5N	0.54%	0.22%	0.25%	0.74%
C10H19O6N	0.48%	1.14%	1.04%	0.86%
C11H19O6N	0.27%	0.32%	0.42%	0.51%
		$CHON_2$		
C4H8O8N2	1.07%	NaN	0.88%	0.54%
C5H8O8N2	1.04%	NaN	4.80%	0.77%
C6H10O8N2	1.38%	1.89%	2.37%	1.38%
C6H10O9N2	0.77%	0.83%	0.81%	0.57%
C6H12O7N2	4.07%	2.54%	NaN	2.43%
C7H12O8N2	1.39%	1.55%	1.58%	1.15%
C7H12O9N2	0.37%	0.59%	0.45%	0.41%
C7H14O7N2	3.31%	1.71%	0.39%	1.98%
C7H14O8N2	0.38%	0.36%	0.35%	0.39%
C8H14O8N2	1.64%	2.43%	1.82%	1.10%
C8H16O7N2	2.60%	1.38%	0.37%	1.91%
C8H16O8N2	0.25%	0.59%	0.35%	0.32%
C9H16O8N2	1.14%	1.40%	1.28%	1.03%
C9H18O7N2	1.85%	0.65%	0.22%	1.07%
C10H18O8N2	0.76%	1.67%	1.95%	1.20%
C10H20O7N2	0.97%	0.41%	NaN	0.55%
C11H22O7N2	0.59%	0.27%	0.19%	0.69%
C12H24O7N2	0.32%	0.32%	0.14%	0.47%
C13H26O7N2	0.14%	0.20%	0.12%	0.26%
C14H28O7N2	0.07%	0.13%	0.10%	0.16%
$C_nH_{2n}O_7N_2$ (n=6-14)	14.15%	7.75%	1.68%	9.74%

Table S11. Volatility of each $C_nH_{2n}O_7N_2$ OOM molecule in winter.

Formula	Volatitliy	Volatility Type
$C_6H_{12}O_7N_2$	3.33	IVOC
$C_7H_{14}O_7N_2$	2.91	
$C_8H_{16}O_7N_2$	2.48	SVOC
$C_9H_{18}O_7N_2$	2.05	
$C_{10}H_{20}O_7N_2$	1.61	
$C_{11}H_{22}O_7N_2$	1.16	
$C_{12}H_{24}O_7N_2$	0.72	
$C_{13}H_{26}O_7N_2$	0.26	
$C_{14}H_{28}O_7N_2$	-0.19	

Table S12. Concentrations of aromatic and aliphatic OOMs in Beijing and other Chinese megacities.

Measurement Site	Time Period	Aromatic OOMs (cm^{-3})	Aliphatic OOMs (cm^{-3})	Reference
Beijing, China	2019 Jan.-Feb.	1.0×10^7	1.1×10^7	This study
	2019 Mar.-Apr.	2.8×10^7	2.5×10^7	
	2019 July-Aug.	4.7×10^7	4.3×10^7	
	2019 Oct.-Nov.	3.0×10^7	3.4×10^7	
Hong Kong, China	2018 Nov.	8.1×10^7	9.7×10^7	2022, Nie et al.
Shanghai, China	2018 Nov.	3.2×10^7	3.0×10^7	2022, Nie et al.
Nanjing, China	2018 Nov.	2.5×10^7	3.7×10^7	2022, Nie et al.

Table S13. Common aromatic and aliphatic OOM molecules in this study and reported in Liu et al. (Liu et al., 2021).

Aromatic OOMs	Aliphatic OOMs
$C_{6-8}H_{8-12}O_4$	
$C_8H_{11}O_{6-8}N$	$C_{5-7}H_{7-11}O_6N$
$C_9H_{17}O_{7,8}N$	$C_6H_{11}O_6N$
$C_{10}H_{15}O_8N$	
$C_8H_{12}O_{10}N_2$	$C_{6-10}H_{10-18}O_8N_2$

Table S14. Median concentrations of ELVOCs, LVOCs and SVOCs of total OOMs in four seasons.

Season	ELVOCs (cm^{-3})	LVOCs (cm^{-3})	SVOCs (cm^{-3})
Winter	1.4×10^6	9.4×10^6	5.3×10^6
Spring	8.6×10^6	2.0×10^7	1.5×10^7
Summer	1.3×10^7	4.0×10^7	8.4×10^7
Autumn	9.6×10^6	2.8×10^7	2.9×10^7

Table S15. Volatility distribution of source-classified OOMs in four seasons.

Season	OOMs Type	ELVOCs + LVOCs	SVOCs	IVOCs + VOCs
Winter	IP OOMs	42.1 %	56.3 %	1.6 %
	MT OOMs	100.0 %	0.0 %	0.0 %
	Aromatic OOMs	77.5 %	13.4 %	9.1 %
	Aliphatic OOMs	54.7 %	38.2 %	7.1 %
Spring	IP OOMs	25.2 %	56.2 %	18.5 %
	MT OOMs	95.7 %	4.3 %	0.0 %
	Aromatic OOMs	69.3 %	21.2 %	9.6 %
	Aliphatic OOMs	38.2 %	50.5 %	11.3 %
Summer	IP OOMs	3.3 %	92.2 %	4.5 %
	MT OOMs	70.9 %	29.1 %	0.0 %
	Aromatic OOMs	73.8 %	20.8 %	5.4 %
	Aliphatic OOMs	17.8 %	71.5 %	10.7 %
Autumn	IP OOMs	15.8 %	48.1 %	36.1 %
	MT OOMs	93.6 %	6.4 %	0.0 %
	Aromatic OOMs	66.7 %	21.6 %	11.7 %
	Aliphatic OOMs	30.0 %	62.0 %	8.0 %

REFERENCES

Atkinson, R., and Arey, J.: Atmospheric Degradation of Volatile Organic Compounds, Chemical Reviews, 103, 4605-4638, 10.1021/cr0206420, 2003.

Dada, L., Paasonen, P., Nieminen, T., Buenrostro Mazon, S., Kontkanen, J., Peräkylä, O., Lehtipalo, K., Hussein, T., Petäjä, T., Kerminen, V. M., Bäck, J., and Kulmala, M.: Long-term analysis of clear-sky new particle formation events and nonevents in Hyytiälä, Atmos. Chem. Phys., 17, 6227-6241, 10.5194/acp-17-6227-2017, 2017.

Donahue, N. M., Robinson, A. L., Stanier, C. O., and Pandis, S. N.: Coupled Partitioning, Dilution, and Chemical Aging of Semivolatile Organics, Environmental Science & Technology, 40, 2635-2643, 10.1021/es052297c, 2006.

Donahue, N. M., Epstein, S. A., Pandis, S. N., and Robinson, A. L.: A two-dimensional volatility basis set: 1. organic-aerosol mixing thermodynamics, Atmos. Chem. Phys., 11, 3303-3318, 10.5194/acp-11-3303-2011, 2011.

Donahue, N. M., Kroll, J. H., Pandis, S. N., and Robinson, A. L.: A two-dimensional volatility basis set – Part 2: Diagnostics of organic-aerosol evolution, Atmos. Chem. Phys., 12, 615-634, 10.5194/acp-12-615-2012, 2012.

Ehn, M., Thornton, J. A., Kleist, E., Sipilä, M., Junninen, H., Pullinen, I., Springer, M., Rubach, F., Tillmann, R., Lee, B., Lopez-Hilfiker, F., Andres, S., Acir, I.-H., Rissanen, M., Jokinen, T., Schobesberger, S., Kangasluoma, J., Kontkanen, J., Nieminen, T., Kurtén, T., Nielsen, L. B., Jørgensen, S., Kjaergaard, H. G., Canagaratna, M., Maso, M. D., Berndt, T., Petäjä, T., Wahner, A., Kerminen, V.-M., Kulmala, M., Worsnop, D. R., Wildt, J., and Mentel, T. F.: A large source of low-volatility secondary organic aerosol, Nature, 506, 476-479, 10.1038/nature13032, 2014.

Epstein, S. A., Riipinen, I., and Donahue, N. M.: A Semiempirical Correlation between Enthalpy of Vaporization and Saturation Concentration for Organic Aerosol, Environmental Science & Technology, 44, 743-748, 10.1021/es902497z, 2010.

Garmash, O., Rissanen, M. P., Pullinen, I., Schmitt, S., Kausiala, O., Tillmann, R., Zhao, D., Percival, C., Bannan, T. J., Priestley, M., Hallquist, A. M., Kleist, E., Kiendler-Scharr, A., Hallquist, M., Berndt, T., McFiggans, G., Wildt, J., Mentel, T., and Ehn, M.: Multi-generation OH oxidation as a source for highly oxygenated organic molecules from aromatics, Atmospheric Chemistry and Physics, 20, 515-537, 10.5194/acp-20-515-2020, 2020.

Liu, Y., Nie, W., Li, Y., Ge, D., Liu, C., Xu, Z., Chen, L., Wang, T., Wang, L., Sun, P., Qi, X., Wang, J., Xu, Z., Yuan, J., Yan, C., Zhang, Y., Huang, D., Wang, Z., Donahue, N. M., Worsnop, D., Chi, X., Ehn, M., and Ding, A.: Formation of condensable organic vapors from anthropogenic and biogenic VOCs is strongly perturbed by NOx in eastern China, Atmos. Chem. Phys. Discuss., 2021, 1-44, 10.5194/acp-2021-364, 2021.

Ma, X., Tan, Z., Lu, K., Yang, X., Liu, Y., Li, S., Li, X., Chen, S., Novelli, A., Cho, C., Zeng, L., Wahner, A., and Zhang, Y.: Winter photochemistry in Beijing: Observation and model simulation of OH and HO2 radicals at an urban site, Science of The Total Environment, 685, 85-95, https://doi.org/10.1016/j.scitotenv.2019.05.329, 2019.

Massoli, P., Stark, H., Canagaratna, M. R., Krechmer, J. E., Xu, L., Ng, N. L., Mauldin, R. L., Yan, C., Kimmel, J., Misztal, P. K., Jimenez, J. L., Jayne, J. T., and Worsnop, D. R.: Ambient Measurements of Highly Oxidized Gas-Phase

Molecules during the Southern Oxidant and Aerosol Study (SOAS) 2013, ACS Earth and Space Chemistry, 2, 653-672, 10.1021/acsearthspacechem.8b00028, 2018.

Molteni, U., Bianchi, F., Klein, F., El Haddad, I., Frege, C., Rossi, M. J., Dommen, J., and Baltensperger, U.: Formation of highly oxygenated organic molecules from aromatic compounds, Atmos. Chem. Phys., 18, 1909-1921, 10.5194/acp-18-1909-2018, 2018.

Seinfeld, J. H., and Pandis, S. N.: Atmospheric chemistry and physics: from air pollution to climate change, John Wiley & Sons, 2016.

Stolzenburg, D., Fischer, L., Vogel, A. L., Heinritzi, M., Schervish, M., Simon, M., Wagner, A. C., Dada, L., Ahonen, L. R., Amorim, A., Baccarini, A., Bauer, P. S., Baumgartner, B., Bergen, A., Bianchi, F., Breitenlechner, M., Brilke, S., Buenrostro Mazon, S., Chen, D., Dias, A., Draper, D. C., Duplissy, J., El Haddad, I., Finkenzeller, H., Frege, C., Fuchs, C., Garmash, O., Gordon, H., He, X., Helm, J., Hofbauer, V., Hoyle, C. R., Kim, C., Kirkby, J., Kontkanen, J., Kürten, A., Lampilahti, J., Lawler, M., Lehtipalo, K., Leiminger, M., Mai, H., Mathot, S., Mentler, B., Molteni, U., Nie, W., Nieminen, T., Nowak, J. B., Ojdanic, A., Onnela, A., Passananti, M., Petäjä, T., Quéléver, L. L. J., Rissanen, M. P., Sarnela, N., Schallhart, S., Tauber, C., Tomé, A., Wagner, R., Wang, M., Weitz, L., Wimmer, D., Xiao, M., Yan, C., Ye, P., Zha, Q., Baltensperger, U., Curtius, J., Dommen, J., Flagan, R. C., Kulmala, M., Smith, J. N., Worsnop, D. R., Hansel, A., Donahue, N. M., and Winkler, P. M.: Rapid growth of organic aerosol nanoparticles over a wide tropospheric temperature range, Proceedings of the National Academy of Sciences, 115, 9122, 10.1073/pnas.1807604115, 2018.

Tan, Z., Fuchs, H., Lu, K., Hofzumahaus, A., Bohn, B., Broch, S., Dong, H., Gomm, S., Häseler, R., He, L., Holland, F., Li, X., Liu, Y., Lu, S., Rohrer, F., Shao, M., Wang, B., Wang, M., Wu, Y., Zeng, L., Zhang, Y., Wahner, A., and Zhang, Y.: Radical chemistry at a rural site (Wangdu) in the North China Plain: observation and model calculations of OH, HO2 and RO2 radicals, Atmos. Chem. Phys., 17, 663-690, 10.5194/acp-17-663-2017, 2017.

Tan, Z., Rohrer, F., Lu, K., Ma, X., Bohn, B., Broch, S., Dong, H., Fuchs, H., Gkatzelis, G. I., Hofzumahaus, A., Holland, F., Li, X., Liu, Y., Liu, Y., Novelli, A., Shao, M., Wang, H., Wu, Y., Zeng, L., Hu, M., Kiendler-Scharr, A., Wahner, A., and Zhang, Y.: Wintertime photochemistry in Beijing: observations of ROx radical concentrations in the North China Plain during the BEST-ONE campaign, Atmos. Chem. Phys., 18, 12391-12411, 10.5194/acp-18-12391-2018, 2018.

Tröstl, J., Chuang, W. K., Gordon, H., Heinritzi, M., Yan, C., Molteni, U., Ahlm, L., Frege, C., Bianchi, F., Wagner, R., Simon, M., Lehtipalo, K., Williamson, C., Craven, J. S., Duplissy, J., Adamov, A., Almeida, J., Bernhammer, A.-K., Breitenlechner, M., Brilke, S., Dias, A., Ehrhart, S., Flagan, R. C., Franchin, A., Fuchs, C., Guida, R., Gysel, M., Hansel, A., Hoyle, C. R., Jokinen, T., Junninen, H., Kangasluoma, J., Keskinen, H., Kim, J., Krapf, M., Kürten, A., Laaksonen, A., Lawler, M., Leiminger, M., Mathot, S., Möhler, O., Nieminen, T., Onnela, A., Petäjä, T., Piel, F. M., Miettinen, P., Rissanen, M. P., Rondo, L., Sarnela, N., Schobesberger, S., Sengupta, K., Sipilä, M., Smith, J. N., Steiner, G., Tomè, A., Virtanen, A., Wagner, A. C., Weingartner, E., Wimmer, D., Winkler, P. M., Ye, P., Carslaw, K. S., Curtius, J., Dommen, J., Kirkby, J., Kulmala, M., Riipinen, I., Worsnop, D. R., Donahue, N. M., and Baltensperger, U.: The role of low-volatility organic compounds in initial particle growth in the atmosphere, Nature, 533, 527-531, 10.1038/nature18271, 2016.

Wang, H., Lu, K., Guo, S., Wu, Z., Shang, D., Tan, Z., Wang, Y., Le Breton, M., Lou, S., Tang, M., Wu, Y., Zhu, W., Zheng, J., Zeng, L., Hallquist, M., Hu, M., and Zhang, Y.: Efficient N2O5 uptake and NO3 oxidation in the outflow of urban Beijing, Atmos. Chem. Phys., 18, 9705-9721, 10.5194/acp-18-9705-2018, 2018.

Wang, M., Chen, D., Xiao, M., Ye, Q., Stolzenburg, D., Hofbauer, V., Ye, P., Vogel, A. L., Mauldin, R. L., Amorim, A., Baccarini, A., Baumgartner, B., Brilke, S., Dada, L., Dias, A., Duplissy, J., Finkenzeller, H., Garmash, O., He, X.-C., Hoyle, C. R., Kim, C., Kvashnin, A., Lehtipalo, K., Fischer, L., Molteni, U., Petäjä, T., Pospisilova, V., Quéléver, L. L. J., Rissanen, M., Simon, M., Tauber, C., Tomé, A., Wagner, A. C., Weitz, L., Volkamer, R., Winkler, P. M., Kirkby, J., Worsnop, D. R., Kulmala, M., Baltensperger, U., Dommen, J., El-Haddad, I., and Donahue, N. M.: Photo-oxidation of Aromatic Hydrocarbons Produces Low-Volatility Organic Compounds, Environmental Science & Technology, 54, 7911-7921, 10.1021/acs.est.0c02100, 2020.

Yan, C., Nie, W., Äijälä, M., Rissanen, M. P., Canagaratna, M. R., Massoli, P., Junninen, H., Jokinen, T., Sarnela, N., Häme, S. A. K., Schobesberger, S., Canonaco, F., Yao, L., Prévôt, A. S. H., Petäjä, T., Kulmala, M., Sipilä, M., Worsnop, D. R., and Ehn, M.: Source characterization of highly oxidized multifunctional compounds in a boreal forest environment using positive matrix factorization, Atmos. Chem. Phys., 16, 12715-12731, 10.5194/acp-16-12715-2016, 2016.